ISSUE: April 2023

Stiff Voltage Clamping Reduces Input Current Ripple In Single-Ended Converters

by Viktor Vogman, Power Conversion Consulting, Olympia, Wash.

In power converters, where the switching transistors are connected in series, energy stored in the transformer leakage inductance can be recycled through the clamping diodes that are an integral part of these architectures. In the "single-ended" topologies, such as forward, flyback, and push-pull, in which the switching transistors are connected to electrical ground, the energy stored in the leakage inductance can be recycled with the help of nondissipative networks (see the reference), providing stiff voltage clamping. These networks contain an additional winding coupled to the ground and a "flying" capacitor connecting identical terminals of the transformer's primary windings and absorbing the energy stored in the leakage inductance.

Besides improving converter efficiency and alleviating problems arising from leakage-inductance spikes, using such an energy recovery technique also opens an opportunity to significantly reduce the current ripple produced by the converter in its primary power delivery path. This ripple reduction associated with continuous current at the converter input can be considered one of the valuable benefits of the mentioned technique because it helps to minimize the size of the input EMI filter.

This article examines processes in the most widely used forward and flyback single-ended topologies with stiff voltage clamping. It provides a framework for making tradeoffs between achieving input current ripple reduction and minimizing transformer winding size.

We begin by reviewing the operation of the stiff clamp technique in the basic forward converter topology. We then see how this technique produces continuous input current, and how the current ripple depends on the magnetic coupling between the primary and secondary windings. We also discuss how the stiff clamp affects the winding size and perform the analysis that helps make tradeoffs between ripple reduction and limiting transformer size.

The details of stiff clamp technique operation in a basic flyback converter are then examined. It is shown that use of this clamping technique can be extended to the flyback topology with a similar benefit of input current ripple reduction as is achieved in the forward topology. Finally, some practical advice is provided on how to implement this technique, including recommendations on positioning of the transformer windings, selection of the type of capacitor most advantageous for the voltage clamping and ripple reduction as well as suggestions on PCB layout for achieving effective peak voltage clamping of the primary-switch.

Input Current Ripple In Stiff Voltage Clamping Converters (Forward Topology)

Let's examine the operation of the stiff clamp technique in the basic forward converter topology providing drain voltage clamping at a 2 x V_{IN} level. It is shown in Fig. 1a.

In addition to the conventional single-ended forward topology this converter incorporates a clamping capacitor C_{CL} connecting identical (in Fig. 1a—undotted) ends of the main w1 and recuperating w2 transformer windings. This capacitor is connected in parallel (via counter-wound windings) with the decoupling cap on the input so that the V_{IN} decoupling function can be shared among the two caps. The clamping cap is always charged to the V_{IN} level but floats to different electric potentials depending on the state of the switch Q1 connected to its positive plate.

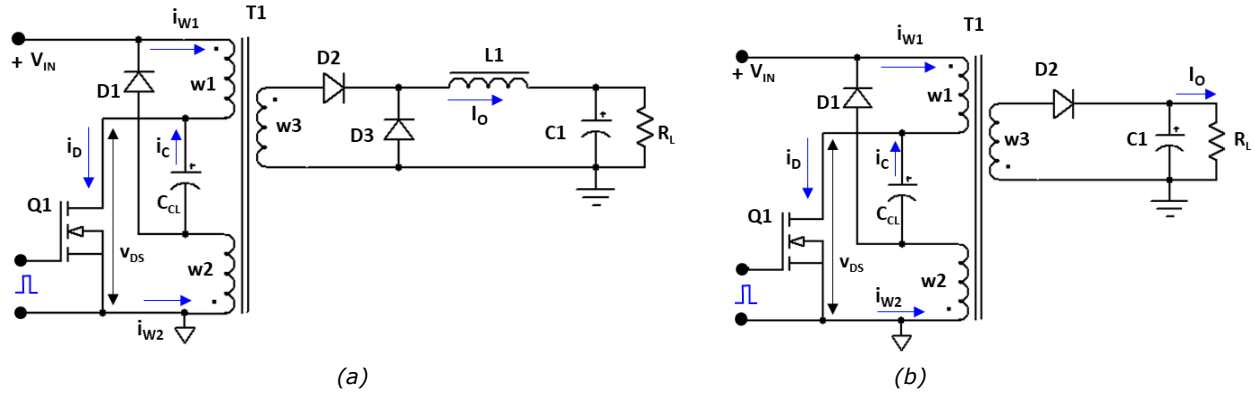

Fig. 1. Forward (a) and flyback (b) single-ended converters with stiff drain voltage clamping at 2 x V_{IN} level.

In the conventional forward converter (not incorporating C_{CL}) during switch on-time, all the energy is transferred to the secondary side via a primary winding w1. The recuperating winding w2 conducts a very small magnetizing current i_μ after the primary switch turns off and is used just for the transformer reset. The timing diagrams in the conventional topology are shown in Fig. 2a.

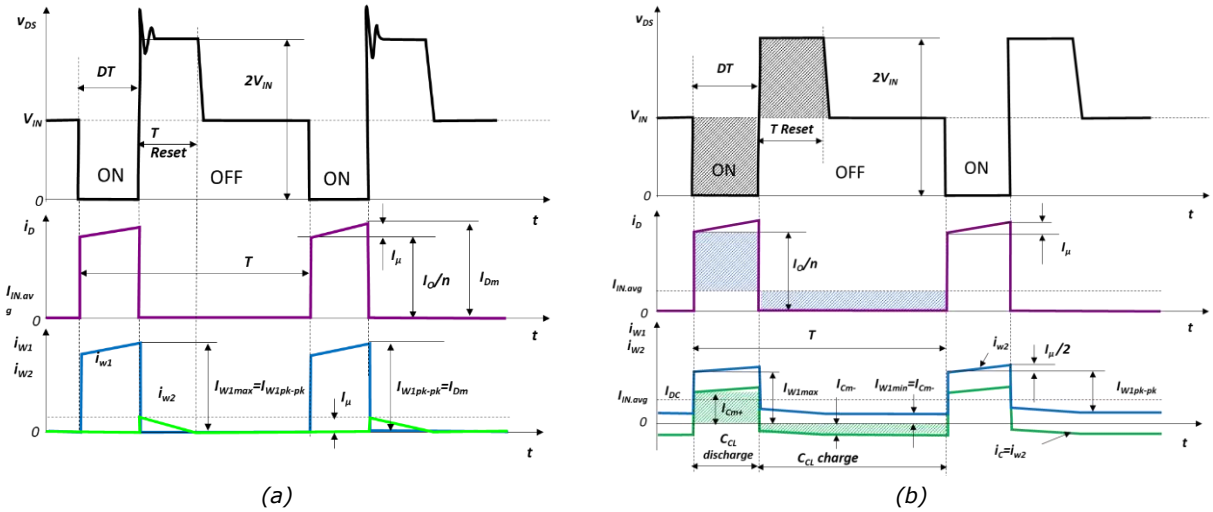

Fig. 2 Voltage and current waveforms in the conventional forward converter (a) and in the stiff clamp forward converter shown in Fig. 1b (b). In these diagrams, the output inductor value is assumed large enough that its impact on the primary-side current ripple can be neglected.

In the current waveforms the output inductor value is assumed large enough that its impact on the primary-side current ripple can be neglected. The set of timing diagrams for the converter with stiff voltage clamping is given in Fig. 2b with reference to Fig. 1a circuit designations.

In the converter with stiff voltage clamping shown in Fig. 1a, the second primary winding w2 creates a path for transferring a portion of energy to the load and the magnetizing current is split between the two primary windings over on and off time intervals. When the switch is on, it connects winding w1 to the primary source V_{IN} and winding w2 to the cap C_{CL}, which is charged to the same voltage level (V_{IN}). The amount of energy that gets delivered to the secondary side via each of the primary windings determines the current magnitudes through the clamping cap C_{CL} and the waveshape of the current drawn from the primary source.

To determine these current magnitudes let's assume for clarity that the magnetizing inductance of the transformer winding is also large enough that the magnetizing current magnitude can be neglected as compared to the components constituting the load current. This assumption will allow us to "rectangularize" the wave shapes and to get simplified analytical expressions having clear physical meaning and providing sufficient accuracy for qualitative analysis.

When Q1 is on (interval DT in Fig. 2b), its drain current is made up of two components: winding w1 current magnitude I_{w1max} and w2 current magnitude I_{w2max} equal to the C_{CL} discharge current magnitude I_{Cm+} (Fig. 2b). When Q1 is off, the clamping cap gets charged with current $i_c = I_{Cm-}$ flowing through back-to-back (counter-wound) primary windings w1 and w2 generating flux in the transformer core in opposite directions.

As can be seen from the circuit in Fig. 1a and waveforms in Fig. 2b, charging the cap during the Q1 off state prevents the primary winding current from dropping to zero, as it occurs in the conventional topology (blue color waveform in Fig. 2a). This continuous input current mode operation makes it relevant to take a closer look at this phenomenon to find out what factors affect the current ripple magnitude ($i_{w1pk-pk}$ in Fig. 2b) and to find out if the primary current ripple can be further smoothed.

Equivalent Circuits And Basic Equations

To quantify the input current ripple, the equivalent converter circuits need to be created for each of the stages of converter operation. These circuits are given in Fig. 3 for Q1 on, and Q1 off, i.e. transformer reset and C_{CL} charge time intervals.

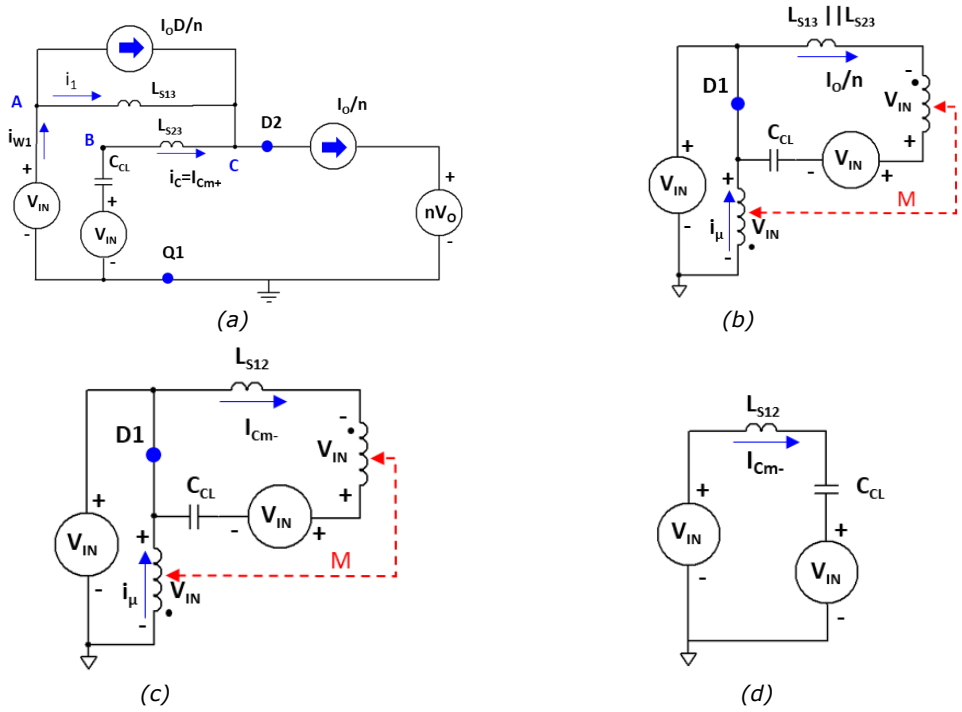

Fig. 3. Converter equivalent schematics for switch-on (a) and switch-off (b , c and d) time intervals. Current i_1 represents the ac component of the primary winding current that gets driven to the output. Once the leakage inductance energy is absorbed by the cap (b), and the transformer reset via D1 (c) is complete, the clamp capacitor charge continues through leakage inductance L_{S12} between two primary windings (d).

As follows from the on-state equivalent circuit shown in Fig. 3a, the energy supplied to the load is delivered via three paths—by a dc current source I_OD/n, representing a dc current component flowing only through the

primary winding w1, and two branches incorporating series leakage inductances L_{S13} and L_{S23} characterizing non-unity magnetic couplings to the secondary winding w3. With reference to the Fig. 3a circuit designations, for node C we can write the following equation according to the first Kirchhoff law:

$$I_{1m}n + I_{Cm+}n = I_O - I_O D \qquad (1)$$

where I_{1m} represents the magnitude of the ac component of the primary winding current i_1 (Fig. 3a), n is the transformer turns ratio, $n = w_1/w_3 = w_2/w_3$ and D is the duty ratio of generated pulses.

Since the capacitor voltage equals V_{IN} and the capacitance is large enough that its voltage change during the pulse top is negligible, points A and B in Fig. 3a circuit are equipotential and can be directly tied without affecting the circuit operation. This connects the leakage inductances L_{S13} and L_{S23} in parallel and makes valid the following equation for the ratio of their current magnitudes:

$$I_{1m}/I_{Cm+} = L_{S23}/L_{S13} \qquad (2)$$

By solving equations (1) and (2) together we can determine the magnitudes of the currents flowing in the two branches:

$$I_{Cm+} = \frac{I_O(1-D)}{n(1+L_{S23}/L_{S13})} \qquad (3)$$

$$I_{1m} = \frac{I_O(1-D)L_{S23}/L_{S13}}{n(1+L_{S23}/L_{S13})} \qquad (4)$$

As follows from equation 4, the ac component magnitude I_{1m} can be significantly reduced if the magnetic coupling between w2 and w3 is much stronger than between w1 and w3, i.e. if $L_{13} >> L_{23}$. Based on a stipulation that the cap current cannot have a dc component, i.e. by equating the amp-second products for cap discharge (on) and charge (off) time intervals (these areas are highlighted with a dotted texture in the Fig. 2b bottom diagram):

$$I_{Cm+}D = I_{Cm-}(1-D)$$

From this relationship, and using equation 3, we can determine the cap charge current magnitude I_{Cm-} (Fig. 3c and d):

$$I_{Cm-} = \frac{I_{Cm+}D}{(1-D)} = \frac{I_O D}{n(1+L_{S23}/L_{S13})} \qquad (5)$$

When the MOSFET is in the off state its current must be zero. This condition can be achieved only when primary winding current is used for C_{CL} charging only, i.e., $i_{w1.min} = I_{Cm-}$ (Fig. 2b). Thus, peak-to-peak input current ripple, defined as a difference between the maximum winding current $i_{w1.max} = I_O/n - I_{Cm+}$ and the minimum winding current (Fig. 2b), can be determined by using equations (4) and (5):

$$\Delta i_{w1.FWD} = i_{w1.max} - i_{w1.min} = \frac{I_O}{n} - I_{Cm+} - I_{Cm-} = \frac{I_O}{n(1+L_{S13}/L_{S23})} \qquad (6)$$

This equation shows that in the stiff clamp forward topology, the input ripple depends on the magnetic coupling between each of the primary windings and the secondary winding w3. The stronger the coupling between the windings w2 and w3 (lower L_{S23}) and the weaker the coupling between the windings w1 and w3 (larger L_{S13}) the smaller the input current ripple can be achieved.

The chart in Fig. 4a plotted for the pk-pk ripple (equation 6) normalized over the conventional case pk-pk ripple (I_O/n) demonstrates that in the stiff clamping forward converter the current ripple can be influenced by varying

the magnetic coupling between each of the primary windings and the secondary winding. Such influence creates an opportunity for reducing the size of the converter's input EMI filter and its cost.

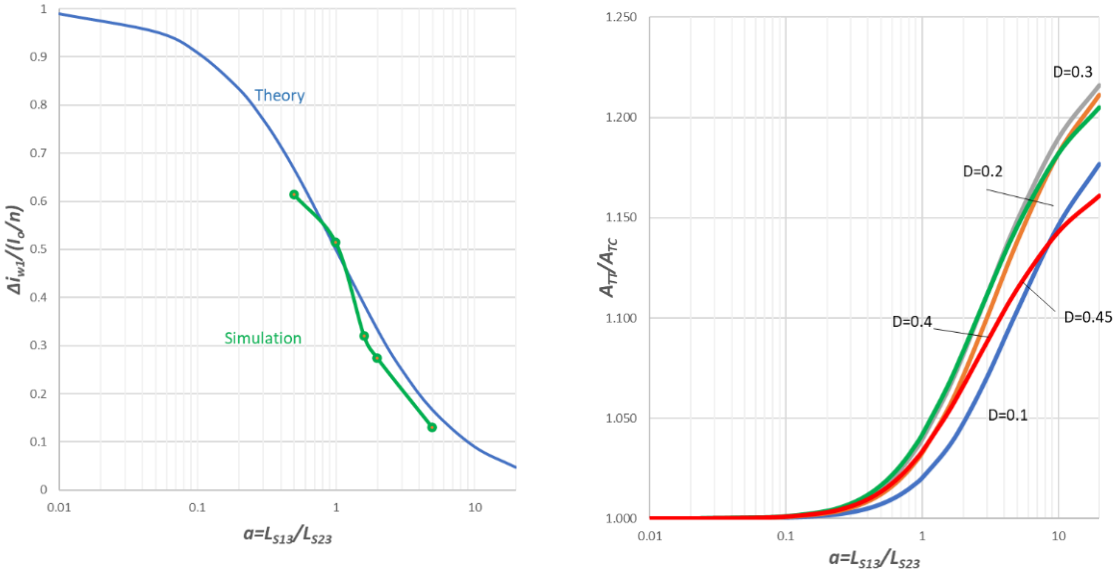

(a) (b)

Fig. 4. Pk-pk input current ripple current (a) and primary winding total cross-sectional area (b) in the stiff clamp converter normalized over the conventional case vs. leakage inductance ratio a = L_{S13}/L_{S23}. Simulation results (green line in diagram a) confirm that the primary current ripple in a stiff clamp forward converter gets reduced with the increase in L_{S13}/L_{S23} leakage inductance ratio according to the prediction (blue line in diagram a). However, the use of the stiff clamp technique has some impact on the primary winding size (b) and designers need to consider the tradeoff between ripple reduction and increased transformer size.

Impact On Transformer Primary Winding Size

The total cross-sectional area of the primary windings is proportional to their RMS currents. In the conventional case, the current in the recuperating winding w2 (i_μ) can be neglected, which is why the total cross-sectional area for the conventional case can be practically defined by the RMS current of the primary winding w1 , the number of turns w on it, and the allowed current density J_i:

$$A_{TC} = \frac{wI_o\sqrt{D}}{J_i} \qquad (7)$$

Assuming the same number of turns in each of the windings for the 2 x V_{IN} clamping case, the total cross-sectional area A_{TT} of the primary windings in the stiff clamp forward converter is

$$A_{TT} = \frac{w}{J_i}\left(I_{w1.RMS} + I_{w2.RMS}\right) \qquad (8)$$

where $I_{w1.RMS}$ and $I_{w2.RMS}$ are the RMS currents in windings w1 and w2, respectively. Knowing the current waveshapes, we can determine the RMS currents in each of the primary windings:

$$I_{w1.RMS.FWD} = \sqrt{\frac{1}{T}\left[\int_0^{DT}\left(\frac{I_O}{n} - I_{Cm+}\right)^2 dt + \int_0^{(1-D)T} I_{Cm-}^2 dt\right]} = \frac{I_O}{n(a+1)}\sqrt{D + 2aD^2 + a^2D^2}$$

$$I_{w2.RMS.FWD} = \sqrt{\frac{1}{T}\left(\int_0^{DT} I_{Cm+}^2 dt + \int_0^{(1-D)T} I_{Cm-}^2 dt\right)} = \frac{aI_O}{n(a+1)}\sqrt{D-D^2}$$

where *a* is the leakage inductance ratio, $a = L_{S13}/L_{S23}$.

These equations can be used for selection of the transformer's primary winding parameters. By substituting these expressions into equations (7) and (8) and considering the cross-section ratio for the stiff clamping and conventional case, A_{TT}/A_{TC}, we can plot the graphs $A_{TT}/A_{TC} = f(a)$ at different duty ratios. These graphs are shown in Fig. 4b.

As can be seen from these graphs the use of the stiff-clamp technique has some impact on the primary winding size and needs to be considered in the tradeoff between increasing ripple reduction versus minimizing transformer size at different L_{S13}/L_{S23} leakage inductance ratios.

Applying The Stiff Clamping Technique To The Flyback Topology

In the flyback converter (Fig. 1b, repeated below in Fig. 5) the operation of the stiff clamp technique providing drain voltage clamping at the 2 x V_{IN} level is very similar to the forward converter case. Voltage and current waveforms in the conventional flyback converter and in its stiff-clamp version are given in Fig. 6a and 6b, respectively. The transformer magnetizing current in the flyback converter topology essentially represents the current supplied to the output referred to the primary side.

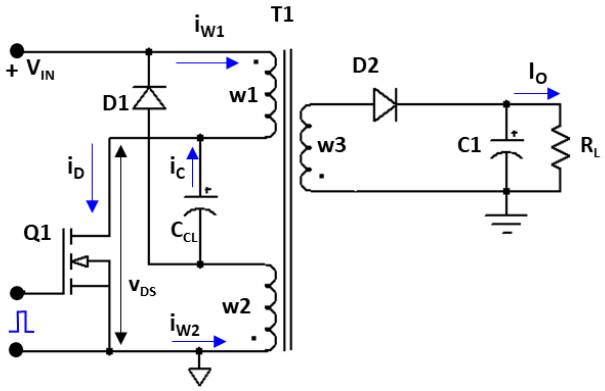

Fig. 5. Flyback single-ended converter with stiff drain voltage clamping at 2 x V_{IN} level.

As with the forward converter case, to get analytical expressions for the component current magnitudes we will be assuming that the magnetizing inductance of the transformer winding is large enough that the slope of the top of the current pulse can be neglected as compared to the current magnitude. The set of diagrams in Fig. 6b represents the "rectangularized" current waveshapes reflecting this assumption.

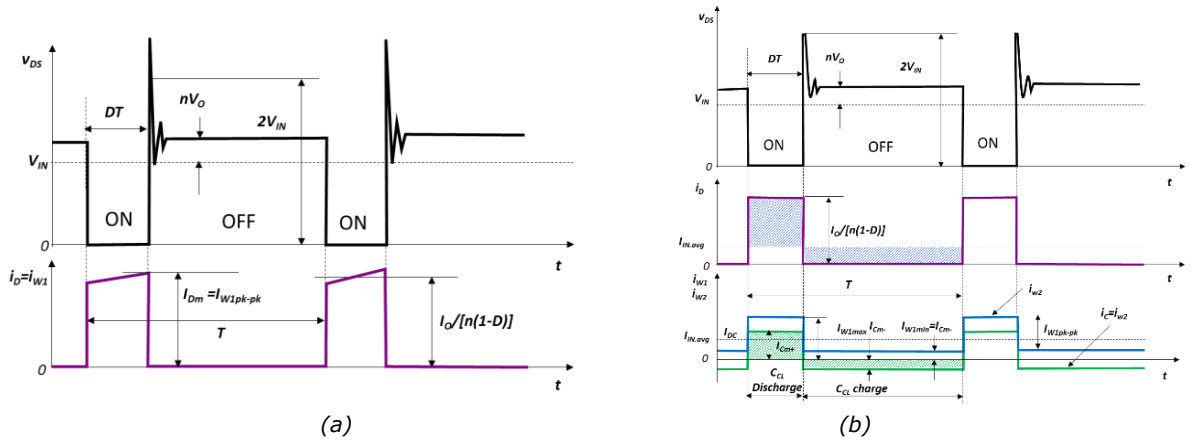

Fig. 6. Voltage and current waveforms in the conventional flyback converter (a) and in the stiff clamp flyback converter shown in Fig. 5 with the current pulse top slopes neglected as compared to the primary current magnitudes (b).

The equivalent converter circuits for each stage of converter operation are shown in Fig. 7.

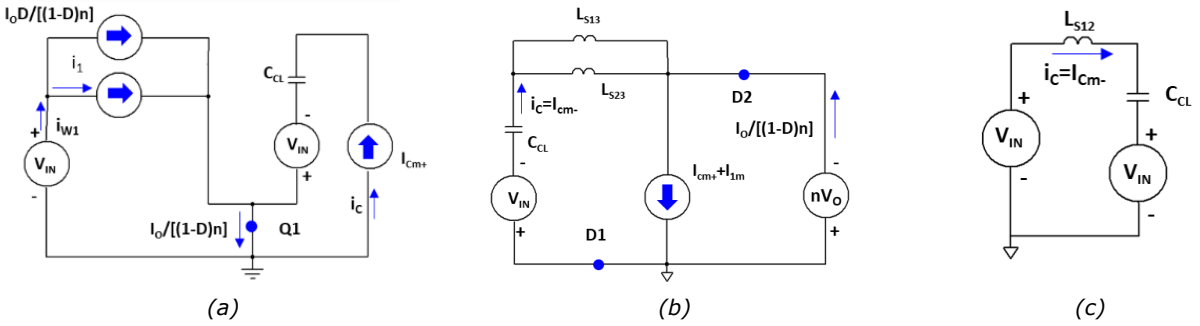

Fig. 7. Flyback converter equivalent circuits for switch-on (a) and switch-off (b and c) time intervals. Q1 current magnitude contains three components—a dc component $I_oD/[(1-D)n]$, ~~and~~ positive peak magnitude I_{1m} in winding w1 and positive cap current peak magnitude I_{Cm+} in winding w2 (a). During the off state, the leakage inductance energy is absorbed by the clamping cap C_{CL}, while the transformer supplies the current $I_o/[(1-D)n]$ to the output (b). The clamp capacitor charge continues via the leakage inductance L_{S12} between two primary windings over a switch-off time interval (c).

Following a similar approach to the forward converter case, solving the equations describing the flyback converter on and off states we find:

$$\Delta i_{w1.FBK} = \frac{I_O}{n(1-D)(1+L_{S13}/L_{S23})} \qquad (9)$$

As can be seen from this equation, the dependence of flyback current ripple on the leakage inductance ratio differs from the forward converter equation 6 by a current magnitude factor (1-D) in the denominator.

By normalizing equation (9) over the conventional flyback converter case pk-pk ripple $I_O/[n(1-D)]$ (Fig. 6a), we can determine that as with the forward converter case, the current ripple in the stiff clamping flyback converter can be controlled by varying magnetic couplings between each of the primary windings and the secondary winding.

That is, the graph of the pk-pk input current ripple current vs. leakage inductance ratio $a = L_{S13}/L_{S23}$ shown in Fig. 4a is fully applicable to the flyback case. The RMS currents in the primary windings can be determined by the following expressions, obtained in a similar fashion to the forward converter case:

$$I_{w1.RMS.FBK} = \frac{I_O}{n(1-D)(a+1)}\sqrt{D + 2aD^2 + a^2D^2}$$

$$I_{w2.RMS.FBK} = \frac{aI_O}{n(1-D)(a+1)}\sqrt{D - D^2}$$

These expressions can be used for selection of the primary winding parameters for the stiff-clamp flyback transformer. Similar to the pk-pk current ripple, the RMS current values also differ from the forward converter case by a current magnitude factor.

After normalizing them over the conventional case primary current magnitude $I_O/[n(1-D)]$ we can conclude that the total impact on relative winding cross-sectional area will be identical to the forward converter case. This means that the graphs in Fig. 4b are also valid for the flyback converter with stiff voltage clamping shown in Fig. 5.

Simulation Results

Simulations of a stiff clamp forward and a stiff clamp flyback converter were performed using a SPICE program. The forward converter simulation was performed for an input supply voltage of V_{IN} = 300 V, duty ratio D = 0.3, V_O = 6 V, I_O = 62 A, and f_{SW} = 100 kHz (T = 10 µs), for the power transformer turns ratio n = 12.9, magnetizing inductance L_μ = 2.5 mH, and a coupling factor between primary windings k_{w1w2} = 0.999.

The flyback converter simulation conditions differed from the forward converter case only by the generated output voltage and current levels due to a larger voltage gain at the same duty ratio: V_O = 9.65 V and I_O = 96 A.

Simulation timing diagrams illustrating the input current ripple reduction phenomenon are shown in Fig. 8a through 8c for the forward converter and Fig. 8d through 8f for the flyback converter.

In these diagrams, the yellow waveforms represent the MOSFET drain current, whose magnitude was kept fixed under all simulation conditions. The current through the clamp capacitor (C = 100 µF) and the primary winding current i_{w1} are represented by green and blue color waveforms for the forward converter and vice versa for the flyback.

These results demonstrate that the primary current ripple in a stiff clamp converter gets reduced with the increase in the L_{S13}/L_{S23} leakage inductance ratio. As noted previously, the simulation results (data points) for a forward converter are also shown for comparison by the green line graph on the chart in Fig. 4a. This comparison confirms that the primary current ripple in a stiff clamp converter gets reduced with the increase in L_{S13}/L_{S23} leakage inductance ratio according to the prediction.

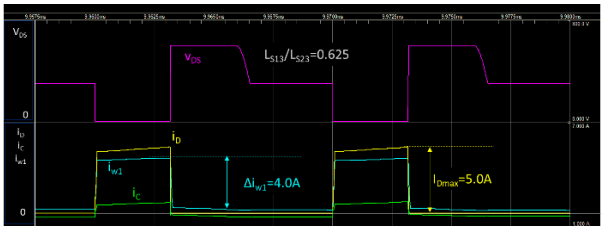

(a) L_{S13}/L_{S23} = 0.625

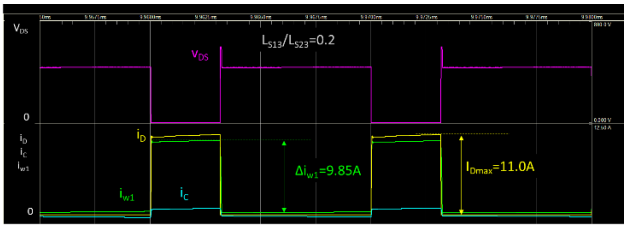

(d) L_{S13}/L_{S23} = 0.2

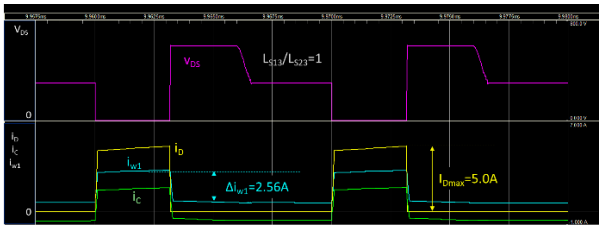

(b) L_{S13}/L_{S23} = 1

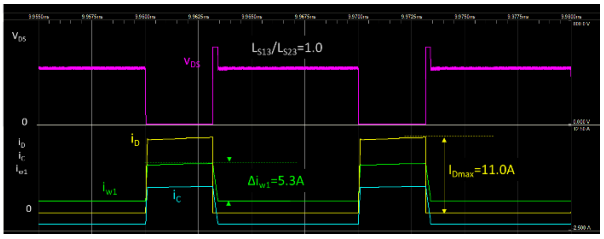

(e) L_{S13}/L_{S23} = 1

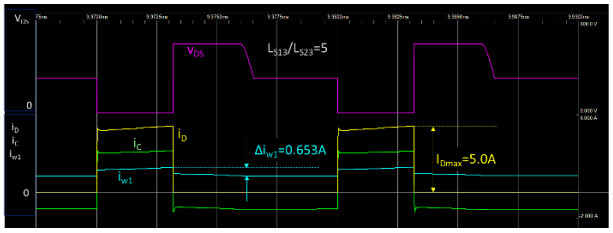

(c) L_{S13}/L_{S23} = 5

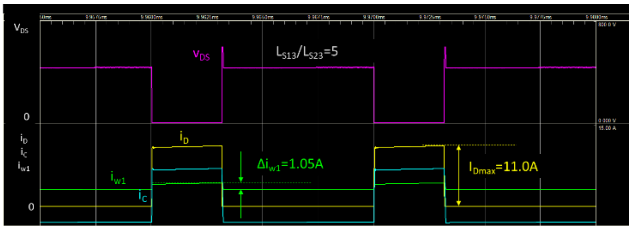

(f) L_{S13}/L_{S23} = 5

Fig. 8. Simulation waveforms for stiff clamp forward (a-c) and flyback (d-f) converters operating at fixed switch current magnitudes, and different L_{S13}/L_{S23} leakage inductance ratios. The results demonstrate that the primary current ripple in stiff clamp converters gets reduced with the increase in L_{S13}/L_{S23} leakage inductance ratio according to the prediction.

Implementation Recommendations

The analysis of stiff voltage clamp converters in each of their operating stages, as presented above, leads us to develop a few recommendations for implementation of this technique. Since ripple reduction in the primary winding lessens the impact of skin effect, a cheaper solid wire can be used for w1 instead of litz wire.

In this type of converter, a leakage inductance increase can be realized by placing a small inductance in series with the primary winding. But the most cost-effective solution would be the integration of L_{S13} into the transformer design. To get a stronger magnetic coupling between w2 and w3 transformer windings, and weaker between w1 and w3, it would be straightforward to position the second primary winding w2 between w1 and w3.

To provide efficient operation of the clamping circuit, components Q1, C_{CL}, D1, and the converter input decoupling cap need to be laid out in the closest proximity to each other. Clamping the drain voltage at a desired level typically requires a relatively small ceramic cap, but for effective reduction of input current ripple using a larger-value electrolytic capacitor is much more efficient. Selecting a larger cap value also reduces the Q-factor in a series L_{S12}-C_{CL} network during the switch-off time interval, assuring its overdamped response.

However, making the clamping capacitance comparable with the bulk cap value can cause an unnecessary increase in the RMS current of the transformer windings because a portion of PFC inductor current, proportional

to the cap value, will be flowing through these windings. This means that the optimal C_{CL} value can be defined as the minimum capacitance that provides an overdamped response in the L_{S12}-C_{CL} network.

Summary

The stiff voltage clamping converter technique examined here is capable of providing significant reduction of input current ripple. The employed converter model using equivalent converter circuits for each of the stages of converter operation and flat-top pulsing current waveforms provides sufficient accuracy for quantifying the effect of leakage inductances on the input current ripple reduction.

The graphs in Fig. 4 illustrating the influence of the stiff voltage clamping converter technique on the input current ripple and transformer winding size can help designers to make tradeoffs between achieving maximum ripple reduction and minimizing transformer size at different L_{S13}/L_{S23} leakage inductance ratios.

The simulation results have been compared with the data obtained with analytical expressions. This comparison has confirmed that the primary current ripple in stiff clamp converter topologies gets reduced with the increase in the L_{S13}/L_{S23} leakage inductance ratio according to the prediction.

Future Work

Additional research could be focused on optimizing the clamp capacitor parameters and developing a procedure for selecting the desired leakage inductance ratio that provides the required noise reduction with an acceptable increase in the size of the transformer's primary winding. Future work could also be concentrated on the evaluation of leakage inductance ratio tolerances and their impact on the design margins that need to be built in when performing converter EMI filter design.

References

"Nondissipative Clamping Benefits DC-DC Converters" by Viktor Vogman, Power Electronics Technology, September 2005, pp. 26-32.

About The Author

Viktor Vogman currently works at Power Conversion Consulting as an analog design engineer, specializing in the design of various power test tools for ac and dc power delivery applications. Prior to this, he spent over 20 years at Intel, focused on hardware engineering and power delivery architectures. Viktor obtained an MS degree in Radio Communication, Television and Multimedia Technology and a PhD in Power Electronics from the Saint Petersburg University of Telecommunications, Russia. Vogman holds over 50 U.S. and foreign patents and has authored over 20 articles on various aspects of power delivery and analog design.

For more on dc-dc converter design, see How2Power's Design Guide, locate the "Power Supply Function" category and select "DC-DC Converters".